MINERALOGICAL MAGAZINE, JUNE 1985, VOL. 49, PP. 375-386

Compositional variation within some sedimentary chlorites and some comments on their origin

C. D. CURTIS, C. R. HUGHES, J. A. WHITEMAN*, AND C. K. WHITTLE

Departments of Geology and Metallurgy*, University of Sheffield, Mappin Street, Sheffield S1 3JD

ABSTRACT. A range of authigenic sedimentary chlorites from sandstones has been studied by analytical transmission electron microscopy. Selected area (single crystal) electron diffraction patterns are of the I*b* ($\beta = 90°$) polytype confirming the earlier observations of Hayes (1970).

TEM analyses show all samples to be relatively rich in both Al and Fe. In the general formula $(Mg,Fe,Al)_n[Si_{8-x}Al_xO_{20}](OH)_{16}$, x varies between 1.5 and 2.6; Fe/(Fe + Mg) between 0.47 and 0.83 and n between 10.80 and 11.54. Octahedral Al is close to 3 in this formulation and Fe^{2+} predominates over Fe^{3+}. Swelling chlorites have significantly different compositions which are consistent with smectite/chlorite interstratifications.

The I*b* ($\beta = 90°$) polytype appears to be stable under conditions of moderate to deep burial. It replaces berthierine and swelling chlorites formed at lower temperatures. As commonly seen in grain coatings, however, it precipitates from porewater; solutes probably being contributed from several mineral decomposition reactions.

KEYWORDS: chlorite, electron microscopy, sandstone, sedimentary rocks.

DEER *et al.* (1962) say of chlorite '. . . principal occurrences are as products of hydrothermal alteration in igneous rocks, in chlorite schists in metamorphic rocks, and together with clay minerals, in argillaceous sediments.' It is deemed to be the most characteristic mineral of the greenschist facies and of both progressive and retrogressive metamorphism of igneous rocks. More recently, perhaps, it has been recognized as a common authigenic constituent of sandstones; very often as beautifully developed framework grain coatings. Chlorite also occurs widely in fine-grained clastic sediments. Studies of clay mineral distribution in present-day oceanic sediments suggest that much may be of detrital origin (Griffin *et al.*, 1968).

Hayes (1970), in a pioneering study, used X-ray diffraction methods in an attempt to distinguish between different chlorite polytypes in sediments and link these with environments of formation. Sedimentary chlorites turned out to be mostly polytype I*b* ($\beta = 90°$) rather than polytype II*b* which is the norm in metamorphic and igneous assemblages (see Bailey and Brown, 1962). Thin section and SEM petrography showed that grain-coating chlorites in sandstones were of undoubtedly authigenic origin and formed at temperatures and pressures much below those of low-grade metamorphism. An evolutionary sequence was proposed starting with highly disordered polytype Ib_d through I*b* ($\beta = 97°$) to I*b* ($\beta = 90°$). Eventually, under conditions approaching those of metamorphism, recrystallization to the most stable polytype II*b* takes place. Little evidence of polytype dependence on chemical composition could be found: temperature was judged to be much more important.

Hayes also estimated chemical composition from unit cell dimensions, observing that 'Because the clay-size chlorites are impure, chemical analysis is useless.' Changes in cell parameters were linked with tetrahedral Al for Si substitution and octahedral Fe for Mg substitution following previously established calibrations (Bailey and Brown, 1962). Complete compositional overlap between diagenetic polytype I and metamorphic polytype II*b* chlorites was documented although the former tended to be somewhat richer in Fe and Al (lower in Si and Mg) than the latter.

Since this work, analytical instrumentation has been developed such that reliable chemical data can be obtained from very small crystals—in polished section by electron microprobe or in ultrathin rock section by analytical transmission electron microscopy. The purpose of the present paper is to follow-up Hayes' (1970) lead with chemical data for sedimentary chlorites obtained by these direct methods and to see if these, when compared with published data for metamorphic chlorites, yield significant information about environments transitional between diagenesis and metamorphism.

Methods and materials

Chemical data. With the exception of wet-chemical Fe^{3+}/Fe^{2+} determinations, all mineral

data were obtained from ultrathin rock sections by ion-beam milling following the techniques of Phakey *et al.* (1972). A Philips 400T analytical TEM/STEM system with EDAX energy-dispersive X-ray analysis was employed. Details have been presented elsewhere (Ireland *et al.*, 1983; Curtis *et al.*, 1984).

The advantages of analytical TEM methods are several. Optical and analytical resolution are much better than in the electon microprobe and this allows data to be taken from single crystals. Selected area diffraction patterns can be obtained at the same time and, if specimen stability allows, a double-tilt stage can yield related series of diffraction patterns.

The combination of very high analytical resolution with excellent observation allows contamination by extremely fine-grain minerals to be identified and (usually) avoided (Curtis *et al.*, 1984). At very high resolution (very small spot size), however, volatile elements may be lost so that the thermal stability of different minerals and elements must be calibrated for specific spot areas. It should also be noted that the analysis system is inferior to the electron microprobe in that counts must be normalized and cannot be evaluated independently.

Once good thin sections have been prepared, it is a relatively simple matter to accumulate large numbers of analyses. The procedure we have adopted is to accept all analyses that meet prior conditions of count-rate and spot area (volatility problem). These are then processed and plotted automatically from data files as molecular propor-

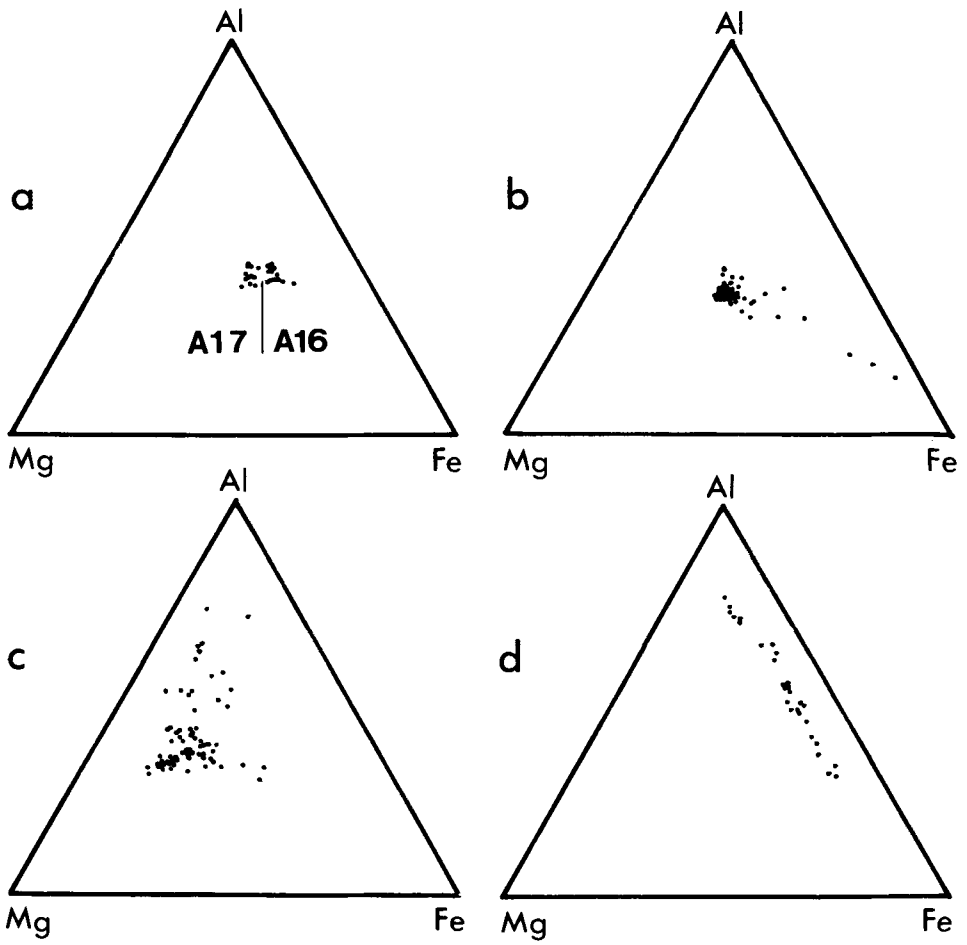

FIG. 1. Individual mineral analyses; various distribution patterns plotted as mol. % element. (*a*) Sandstones A16 and A17 (14 and 15 analyses respectively). (*b*) Sandstone A11, 66 analyses. (*c*) Shale MDT3, 74 analyses. (*d*) Glauconite analyses, 3 sandstones, 33 analyses.

tions on triangular diagrams. Fig. 1 illustrates typical distribution patterns (Al–Mg–Fe): 1*a* plots individual analyses from Falher Formation sandstone samples A16 and A17. Both samples yield tight data point clusters which do not overlap. Scatter is due to the sum of experimental error and between-crystal variation. The latter must be small, therefore, and suggests that a single equilibrium phase may have been analysed in each case. The chlorite grain coatings in these two sandstones, however, have significantly different compositions. For symmetrically distributed data points such as these, a mean analysis provides the best estimate of mineral composition.

In fig. 1*b*, however, some 66 analyses from coating grains in Palaeogene sandstone A11 present a different distribution. There is a tight cluster of data points with low Fe-content but, in addition, a tail towards the Fe corner. Extremely fine-grained iron oxides are visible (TEM) in many sandstone samples and this kind of distribution shows that the analysis spot cannot always be located so as to avoid contamination (Curtis *et al.*, 1984). The plot is thus a mixing curve between the chlorite composition being sought and an iron oxide. There is no entirely rigorous method for separating the two since extreme Fe-poor analyses include a component of analytical scatter. The procedure we have adopted is to identify several analyses representative of the Fe-poor cluster on the Si–Al–Fe plot and also on an Al–Fe–Mg plot. The mean analysis of points common to both groups is then taken to be a reasonable estimate of the silicate composition. These are the data presented in Table I. Occasionally distributions such as that in fig. 1*c* are encountered (chlorite?-bearing shale from the Precambrian Hamersley Group). It seems quite clear that different crystals from a single phase are

TABLE I. Chlorite formulae (basis 20 (O) + 16 (OH) assumed)

	Tuscaloosa sandstone						Falher Fm. sandstones		North Sea sandstones					
	5610 m				2400 m		1970 m							
	A02	A03	A04	A05	A06	A07	A17	A21	B01	B07	B08	B09	B10	B16
Si	6.12	6.20	5.36	5.73	6.24	6.15	5.58	5.88	5.81	5.43	5.45	5.95	5.55	5.34
Al	1.88	1.80	2.64	2.27	1.76	1.85	2.42	2.12	2.19	2.57	2.55	2.05	2.45	2.66
Al	3.04	2.54	3.05	3.53	3.35	2.32	3.02	3.26	3.33	2.74	2.88	3.37	2.80	3.10
Ti	0.01	0.00	0.04	0.02	0.03	0.11	0.03	0.16	0.00	0.00	0.01	0.02	0.00	0.00
Fe^{3+}	0.57	0.47	0.51	0.58	0.54	0.69	0.47	0.45	0.43	0.45	0.51	0.36	0.44	0.39
Fe^{2+}	5.12	4.25	4.56	5.22	4.90	6.22	4.19	4.01	3.84	4.09	4.58	3.25	3.92	3.55
Mn	0.03	0.11	0.01	0.02	0.01	0.00	0.01	0.00	0.00	0.00	0.01	0.00	0.00	0.00
Mg	2.30	3.95	3.17	1.67	2.00	1.46	3.59	3.11	3.55	4.23	3.49	4.01	4.38	4.48
Ca	0.05	0.08	0.08	0.01	0.06	0.30	0.04	0.00	0.03	0.06	0.01	0.00	0.02	0.01
Na	0.00	0.00	0.17	0.00	0.00	0.00	0.10	0.05	0.00	0.06	0.02	0.12	0.07	0.06
K	0.05	0.00	0.02	0.02	0.04	0.42	0.08	0.08	0.09	0.14	0.13	0.17	0.01	0.03
OCT.	11.07	11.32	11.35	11.04	10.83	10.80	11.31	10.99	11.15	11.51	11.48	11.01	11.54	11.52
Fe + Mg	7.99	8.67	8.24	7.47	7.44	8.37	8.25	7.57	7.82	8.77	8.58	7.62	8.74	8.42
Fe/(Fe + Mg)	0.71	0.54	0.62	0.78	0.73	0.83	0.56	0.59	0.55	0.52	0.59	0.47	0.49	0.47

	Alaskan sandstones			Belly River sandstone				Berthierine	Hamersley Group			Cambrian Welsh slate	
				1200 m									
	A10	A10'	A11	A12	A13	A14	A15	FRD	058	065	P45	BL1R	BL2G
Si	6.77	7.94	6.90	6.12	6.49	5.79	5.74	6.09	5.41	5.51	5.67	5.45	5.14
Al	1.23	0.06	1.10	1.88	1.51	2.21	2.26	1.91	2.59	2.49	2.33	2.55	2.86
Al	3.16	4.15	2.97	2.93	2.30	3.53	3.34	1.33	2.42	2.55	1.95	3.06	3.04
Ti	0.03	0.06	0.01	0.02	0.00	0.04	0.01	0.00	0.00	0.01	0.00	0.01	0.00
Fe^{3+}	0.43	0.32	0.36	0.61	0.71	0.50	0.56	1.47	0.56	0.58	0.54	0.34	0.99
Fe^{2+}	3.85	2.88	3.25	5.50	6.41	4.54	5.08	7.36	5.08	5.24	4.87	1.34	3.97
Mn	0.02	0.01	0.10	0.01	0.00	0.01	0.02	0.00	0.00	0.00	0.00	0.24	0.10
Mg	2.92	1.92	3.90	1.97	1.54	2.39	2.11	1.17	3.69	3.21	4.53	6.44	3.18
Ca	0.32	0.29	0.20	0.04	0.23	0.02	0.03	0.17	0.00	0.00	0.01	0.01	0.01
Na	0.04	0.22	0.08	0.07	0.00	0.00	0.00	0.00	0.00	0.13	0.00	0.46	0.19
K	0.08	0.16	0.10	0.04	0.10	0.02	0.01	0.13	0.07	0.03	0.05	0.07	0.03
OCT.	10.41	9.34	10.59	11.04	10.96	11.01	11.12	11.33	11.75	11.59	11.89	11.43	11.28
Fe + Mg	7.2	5.12	7.51	8.08	8.66	7.43	7.75	10.00	9.33	9.03	9.94	8.12	8.14
Fe/(Fe + Mg)	0.59	0.63	0.48	0.76	0.82	0.68	0.73	0.88	0.60	0.64	0.54	0.21	0.61

not being analysed. In such cases a mean analysis has no meaning: an unstable assemblage is present. Occasionally distributions indicating silicate mixing curves are obtained. It is then helpful to take cluster means at different ends of the range: samples A10 and A10′ in Table I are of this type. An extreme example of this is illustrated in fig. 1*d* which plots glauconite analyses obtained by the same techniques (Ireland *et al.*, 1983). In this case, several rock samples are included and variation represents true solid solution.

X-ray diffraction. Clay coatings are separated from framework grains by gently disaggregating and rolling samples under distilled water in agate. Smear mounts were prepared without further grinding or size fractionation (very poorly orientated slides are so obtained). Traces between 3° and 43° 2θ (Cu-$K\alpha$) were taken from air-dry, glycollated and heated (550°, 1 hour) slides in sequence. It should be noted that neither complete expansion with ethylene glycol nor complete contraction on heating would be expected for some of the larger crystals in these samples.

The Tuscaloosa, Belly River, Falher, and North Sea sandstones proved to contain well-crystallized chlorite with 002 reflections most intense (relative intensities 001:002:004 approximately 1:6:3). Zero response to glycollation was observed with slight or zero contraction on heating. Radical alteration of relative peak intensities was seen, however, with 001 enhanced and 002 very much reduced. Basal spacings (17 samples) all fell within the range 14.11 to 14.15 Å (calculated from 004 reflections using quartz as internal standard).

The exceptions to this simple picture were clay coatings from sandstones A10, A11 and, to lesser extent, Belly River sandstone samples A12 and A13 (difficult to evaluate due to preponderance of kaolinite). The 001 reflection was found to be equal to or more intense than the 002 reflection and glycollation caused partial expansion from a single, broad and asymmetric peak in the 14.2 to 14.4 Å region to something in excess of 16 Å together with a peak at 14.1 to 14.2 Å. Heating to 550 °C collapsed the glycollated peak to leave a broad reflection near 14.2 Å. XRD traces from sample A10 were very similar to those described previously from another sample (Curtis *et al.*, 1984; sample E79-1). It was there argued that chemical composition and diffraction data could best be interpreted as intermediate between true chlorite and vermiculite (see also MacEwan and Wilson, 1980). The term swelling chlorite has been frequently used to describe such clays and will be retained here.

Electron diffraction. Good, single crystal diffraction patterns were obtained from a few chlorite grains in appropriate orientations. One of these (Falher Formation sandstone A16; see Curtis *et al.*, 1984) is illustrated in fig. 2. Attempts were made to index this on unit cells quoted in Bailey (1980). The fit is very good indeed for polytype I*b* ($\beta = 90°$), $a = 5.39$, $b = 9.34$, $c = 14.14$ Å, with the indices quoted but the pattern cannot be even remotely well-indexed on a typical polytype II*b* cell ($a = 5.37, b = 9.30, c = 14.19$ Å, $\beta = 97.0°$). Our electron diffraction data are consistent with Hayes' (1970) finding that the majority of authigenic sedimentary chlorites are polytype I*b* ($\beta = 90°$). They are also consistent with basal spacing estimates by X-ray diffraction—all values falling in the range 14.11 to 14.15 Å. It should be stressed, however, that unambiguous polytype identifications by TEM were obtained for only one or two of the samples described here. Where XRD traces were obtained from almost pure chlorite separates, the I*b* ($\beta = 90°$) polytype was invariably indicated.

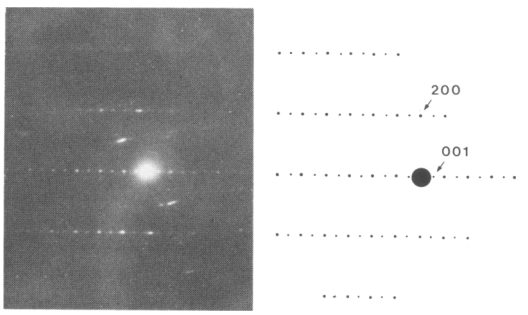

FIG. 2. Selected area diffraction pattern. Chlorite from Falher Formation sandstone. Chlorite polytype I*b* ($\beta = 90°$).

Scanning electron microscopy. The chlorite coatings were examined in the SEM (Philips 500). Fig. 3*a* (Tuscaloosa sandstone—deeply buried) is a good example of well-crystallized authigenic chlorite. Individual crystals are almost perfectly planar and can have euhedral outlines. In other sandstones (fig. 3*b*, Belly River sandstone), crystals are finer and less well developed although still recognizably chlorite. Swelling chlorite is different in appearance. The coatings in sample A11 consist of coarser crystals which are distinctly curved, have irregular outlines and appear to have some kind of surface coating (fig. 3*c*). This is almost certainly hematite: minute iron oxide crystals can be seen in transmission and the analytical data in fig. 1*b* are from this sample. In some areas, the chlorite coatings include numerous small quartz crystals which do not have the common orientation often seen when overgrowth on a framework grain has

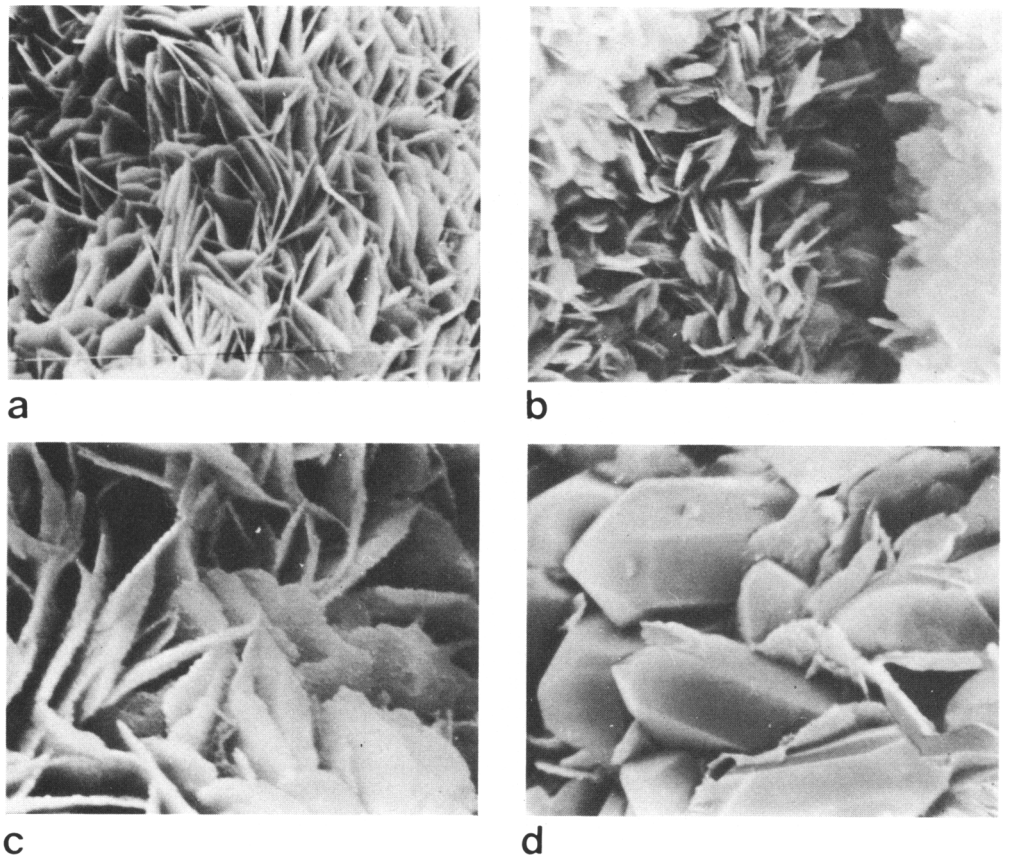

FIG. 3. Scanning electron micrographs. (*a*) A05 Tuscaloosa sandstone: well-crystallized chlorite coatings, (*b*) A12 Belly River sandstone: finer-grained chlorite coatings. (*c*) All 'Swelling chlorite', Alaska: large curved crystals with coatings of ?iron oxides. (*d*) All small quartz crystals with swelling chlorite.

taken place. These are illustrated in fig. 3*d*. Perhaps high degrees of silica supersaturation are implied by this multiple nucleation.

Materials. All sandstone samples were provided, as core, by major oil companies (see acknowledgements). Brief details (in so far as they are known to the authors) are given in the Appendix. Although we were primarily concerned with obviously authigenic grain coatings, we extended our survey to include one or two additional chlorite types which, by virtue of their extremely fine grain size, would also be difficult to analyse by conventional methods. The first of these was the chlorite found in chamositic iron ores (Frodingham Ironstone). It also seemed sensible to look, for comparative purposes, at a few examples of metamorphic chlorites. Here our prime concern was to see if our analytical data would prove to be compatible with previously published analyses and to establish that any differences between diagenetic and metamorphic chlorites could not be attributed to systematic inter-laboratory error. Chlorites from three stilpnomelane-bearing mudrocks from the Hamersley basin were chosen as one group, and chlorites from red (oxidized) and green (reduced) varieties of slate from the Cambrian Slate Belt in Gwynedd for the other (phengite–albite–chlorite–quartz).

Results and discussion

Nomenclature. In accordance with the recommendation of the AIPEA nomenclature committee (AIPEA, 1980), the following are adopted:

GROUP:	chlorite
SUB-GROUP:	trioctahedral, dioctahedral chlorite
TRIOCTAHEDRAL SPECIES:	clinochlore (Mg-rich), chamosite (Fe-rich).

All other varietal names based on composition for common Fe/Mg chlorites are dropped. Berthierine has priority for Fe-rich 1:1 (7.0 Å) sheet silicates with appreciable aluminium (i.e. similar in composition to chamosites). Problems arise here because sedimentologists tend to retain the name chamosite for sedimentary 7 Å chlorites.

Chemical compositions. All the grain-coating chlorites in Table I are relatively rich in both Al and Fe. In the general chlorite formula $(Mg,Fe,Al)_n[Si_{8-x}Al_xO_{20}](OH)_{16}$, our analyses calculate out with x between 1.5 and 2.6, n between 10.80 and 11.54, Fe/(Fe+Mg) between 0.47 and 0.83 and octahedral Al between 2.30 and 3.53. Wet chemical determinations of $Fe^{2+}:Fe^{3+}$ show the former to predominate with values ranging to 9:1. Lower ratios almost certainly reflect the presence of iron oxides. The limiting value is thought to be the best available estimate for the chlorite phase and is *assumed* for all the grain-coating chlorites in Table I. Lower values were obtained for the swelling chlorite samples but it was not possible to establish whether this was entirely due to the presence of oxides.

The octahedral totals are substantially lower than the theoretical 12.0 value for trioctahedral chlorite. Significant vacancies are indicated but, according to Deer *et al.* (1962), many biotites have octahedral totals close to 5.5 (out of a theoretical six) suggesting that vacancies are perhaps to be expected in trioctahedral aluminosilicates.

A useful plot to illustrate compositional variation is tetrahedral Al content (x in the formula above) versus Fe/(Fe+Mg): this was also used in Hayes' (1970) definitive work. Fig. 4 shows variation within the 150-plus chlorite analyses selected from the literature by Foster (1962). They span the complete Mg/Fe substitutional range but are much less variable in tetrahedral Al (with the exception of Mg-rich clinochlores, many fall within the 2.4 to 2.9 interval). 90% of the data points fall within the arbitrary 'box' in fig. 4 leaving a scatter of chamosite analyses with low Al-values.

In fig. 5, we have plotted the two Welsh slate and three stilpnomelane mudrock chlorites. The mudrock and green slate chlorites are chamosites; the red slate chlorite is a clinochlore. At high oxygen partial pressures, the bulk of iron obviously precipitates as hematite leaving little Fe^{2+} available. These data fall well within the range expected for metamorphic chlorites and provide token con-

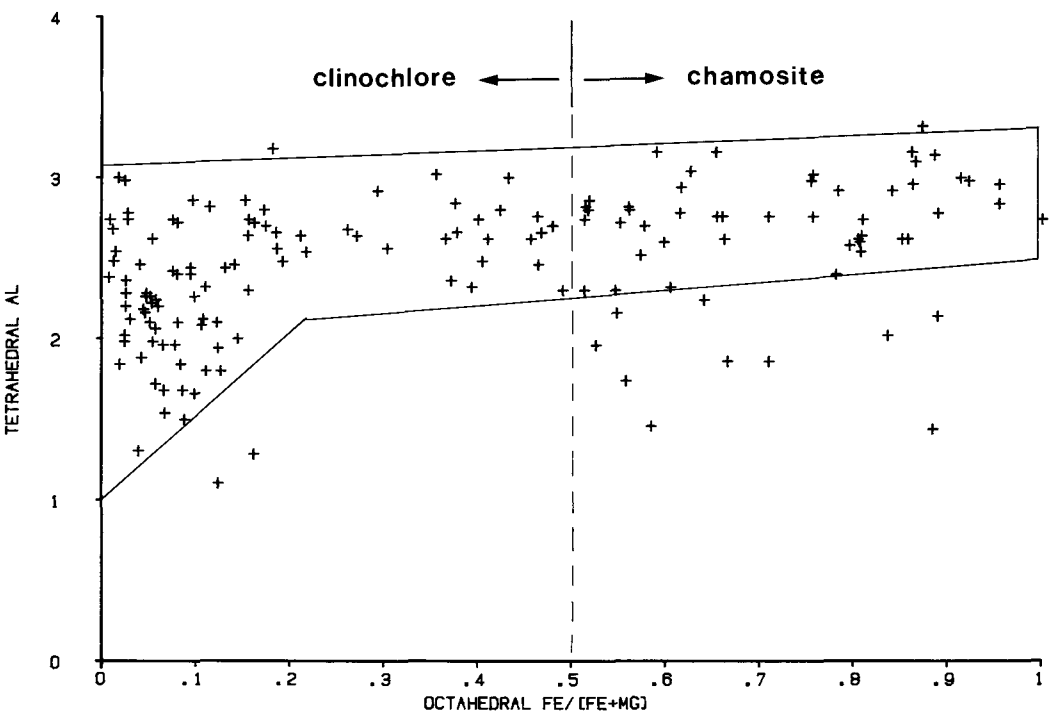

FIG. 4. Chlorite analyses from Foster (1962) plotted as in Hayes (1970). 90% of the analyses plot within the 'box' enclosure; most of those falling outside are Si-rich chamosites.

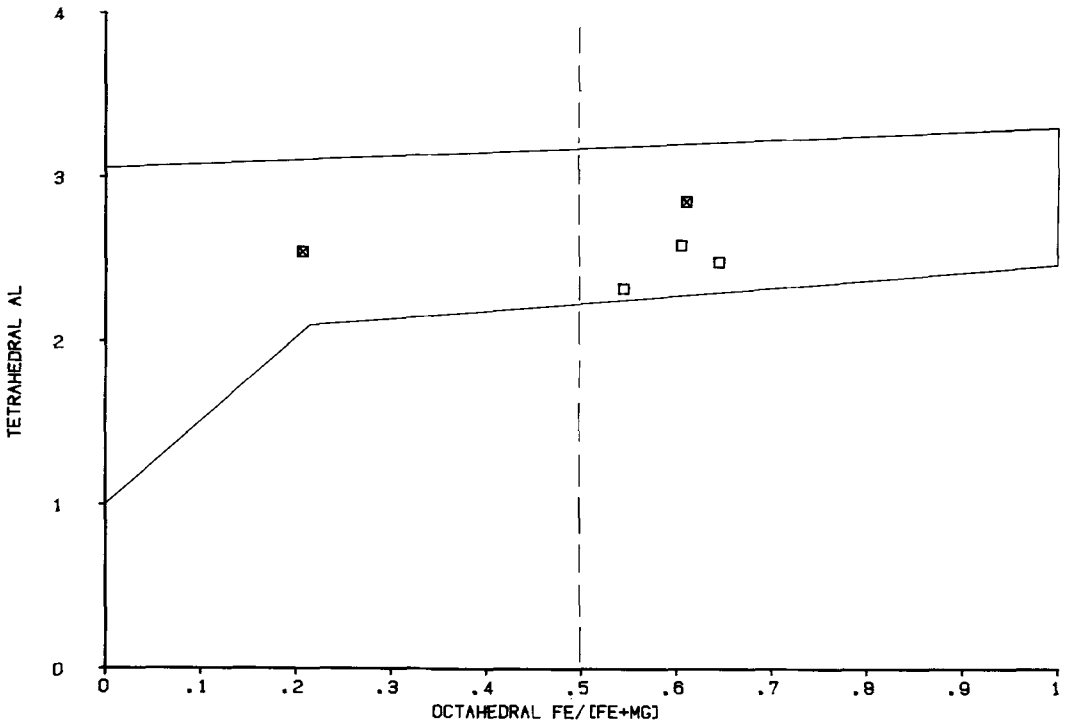

FIG. 5. Analytical TEM data for the Welsh slate and Hamersley stilpnomelane-bearing mudrock chlorites.

firmation of the reliability of our analytical procedures.

Grain-coating polytype I*b* ($\beta = 90°$) chlorites from Table I are plotted in fig. 6, again on the same axes, with Foster's (1962) compositional range for comparison. Most are chamosites and fall outside the central range of Foster's data. Significantly, however, they overlap almost completely with the 'anomalous' Al-poor chamosites in fig. 4. In general, it would appear that authigenic sedimentary chlorites are substantially more ferroan than many, if not most, metamorphic chlorites. Although they are all rich in Al, tetrahedral substitution is lower (all are relatively siliceous). It is tempting to draw a simple analogy with illites which bear the same relationship to phengites.

From these plots, it appears that sedimentary chlorites do differ significantly in composition from polytype II*b* metamorphic chlorites: a conclusion not reached by Hayes (1970) on the basis of X-ray diffraction data. The more direct analytical approach offered by TEM thus suggests that detailed compositional studies are worthwhile and might yield significant information about pore-water composition (especially Mg^{2+}/Fe^{2+} ratios) as well as temperature variation during diagenesis.

The two analyses for swelling chlorite sample A10 represent ends of a compositional range. Individual analyses are probably inter-stratifications of chlorite with vermiculite or smectite in differing proportions. Our data calculation routines, however, assume 36 anion formulae throughout, whereas smectites or vermiculites should be expressed in terms of a 24 anion cell. Incorrectly presenting a smectite analysis as a chlorite formula raises cation values by a factor of 28/22. Spuriously high Si (low tetrahedral Al) and low octahedral totals result. Both are seen in the formula for A10′ which, on the inter-stratification model, should therefore have a large micaceous component. Recalculating this on twenty-two rather than twenty-eight oxygen equivalents gives Si = 6.24, tetrahedral Al = 1.76, octahedral Al = 1.55 and octahedral total 5.63. A 2:1 class mineral of this composition would be an aluminous trioctahedral smectite. The formula for A10 is intermediate between A10′ and typical I*b* ($\beta = 90°$) chlorites already described.

The distribution of our swelling chlorite analyses (fig. 7) thus approximates to a mixing curve between typical I*b* ($\beta = 90°$) chlorite and an aluminous trioctahedral smectite with very similar or even

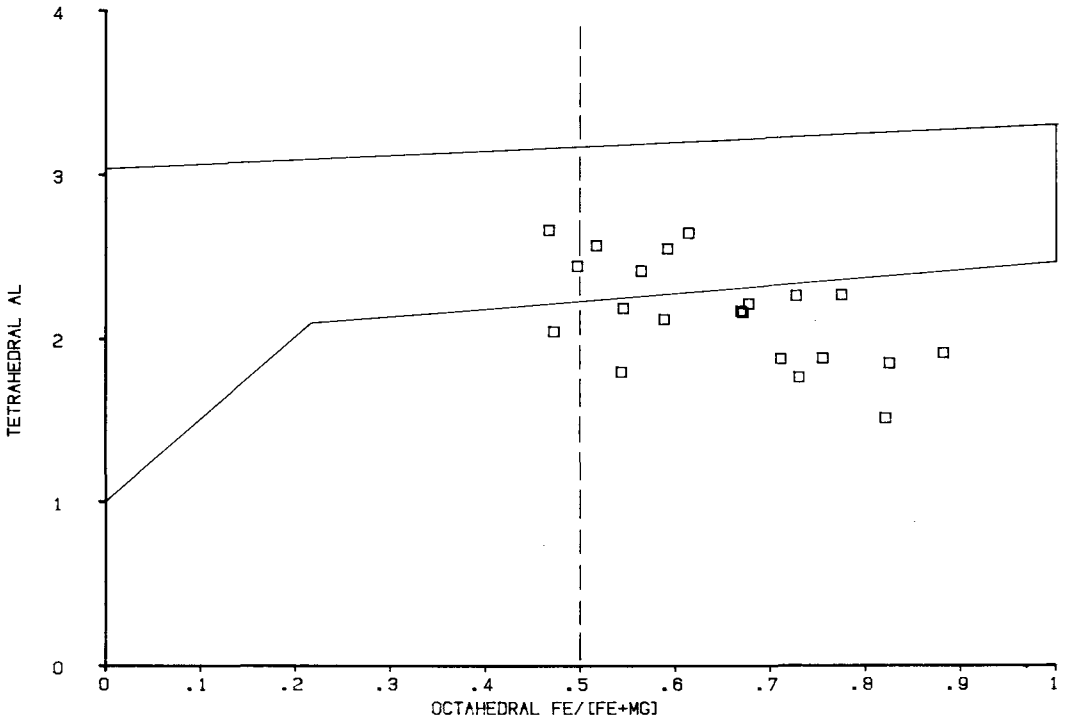

FIG. 6. Analytical TEM data for grain-coating (polytype I*b*?) chlorites.

identical 2 : 1 layer composition. A structural model based on this interstratification has been proposed for a different example by Curtis *et al.* (1984) and is essentially similar to that proposed much earlier by Brindley (1961, p. 286) who envisaged islands of brucite interleaved within a talc-like structure. If this structural model is generally applicable to swelling chlorites, it suggests that they may be intermediates in a diagenetic progression whereby early smectites are converted to chlorite. Late stages in this conversion would leave islands of smectite within a chlorite structure, which offers another possible explanation for low octahedral cation totals. It would also account for small yet significant Ca^{2+}, Na^{+}, or K^{+} concentrations which are consistently indicated by X-ray spectra.

The only berthierine sample (structure confirmed by selected area electron diffraction) analysed here proved to be similar in overall composition to I*b* ($\beta = 90°$) chamosites save for a higher Fe/(Fe + Mg) ratio. This presumably reflects the much greater relative availability of Fe in fine-grained siliclastic sediments where berthierine develops.

Formation and stability of sedimentary chlorites. Relatively few descriptions of sedimentary or fine-grained metamorphic chlorites using modern instrumental methods of analysis have appeared in the literature. Boles and Franks (1979) studied authigenic chlorites in Wilcox (L. Eocene) sandstones of south-west Texas at depths to 4.65 km. Their microprobe analyses were very similar to those reported here and would plot within our sedimentary group in fig. 6. No systematic compositional trends with depth were identified.

McDowell and Elders (1980) analysed authigenic phyllosilicates in sediments in the very high thermal gradients of the Salton Sea Geothermal Field. Microprobe chlorite analyses documented several systematic trends with increasing depth and temperature. Low octahedral totals ($\sim$ 11.0 at 150 °C) at relatively shallow depths approached the theoretical value of 12.0 at 360 °C. A trend from (Fe + Mg) = 7.6 at the lower temperature to 9.7 at 360 °C was documented. It must be presumed that I*b* polytypes would have been recrystallized to II*b* within this temperature range. The I*b* ($\beta = 90°$) polytype analyses in Table I all have relatively low octahedral totals and (Fe + Mg) values between 7.4 and 8.7. These are lower than in the 'hydrothermal' chlorites of McDowell and Elders (1980) and also in microprobe analyses of hydrothermal chlorites reported by Parry and Downey (1982).

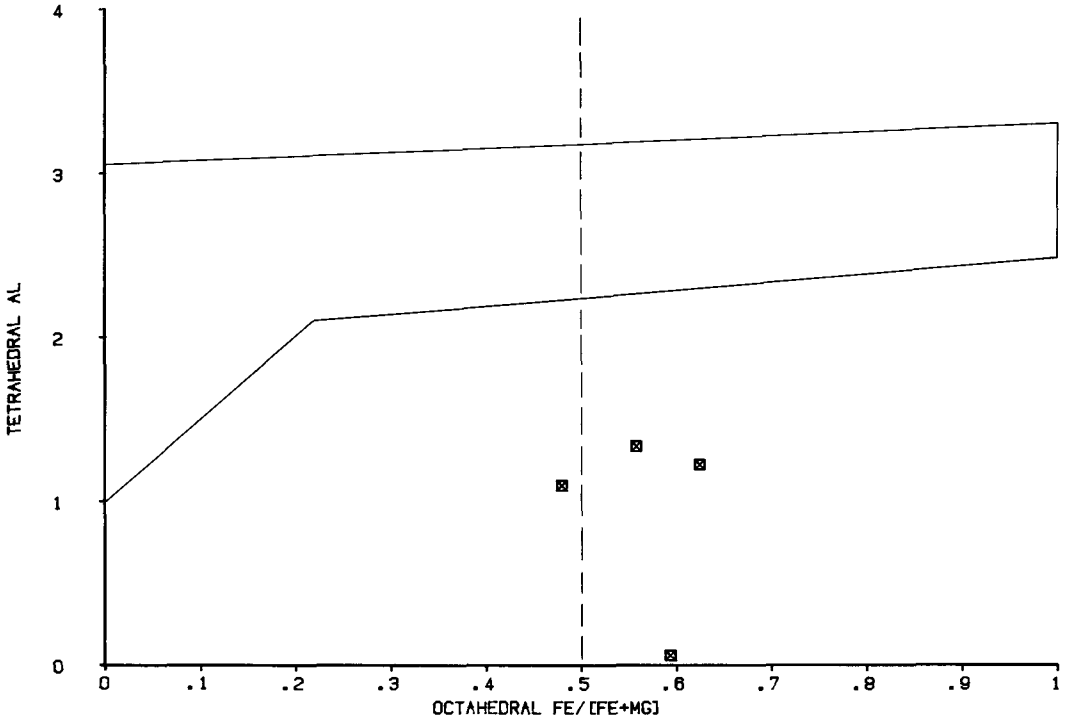

FIG. 7. Analytical TEM data for swelling chlorites.

The very tentative general conclusion that can be drawn from these few comparisons is that true sedimentary chlorites (i.e. those formed at temperatures substantially below 200 °C) have higher Si, lower (Fe + Mg) and lower octahedral totals than those stable at significantly higher temperatures. These differences probably reflect elimination of residual smectite layers. Alternatively, however, it is possible that the tetrahedral sheet composition is modified by incorporation of Al or exclusion of Si. Such a change would be essentially similar to the smectite → illite → phengite progression in mudrock → slate.

Both of the above reports indicate that authigenic 14 Å grain-coating chlorites form under conditions of moderate to deep burial (temperatures near 150 °C), principally at the expense of kaolinite. Several authors (Muffler and White, 1969; Hutcheon *et al.*, 1980) have suggested that carbonate minerals (dolomite, ankerite) are involved in this reaction with calcite and CO_2 as additional products.

Much less is known about authigenic chlorites in fine-grained siliciclastic sediments. 7 Å berthierines are not uncommon in certain types of Fe-rich mudrock and may constitute the bulk of the sediment. The suggestion that their composition is broadly similar to authigenic 14 Å chamosites (Table I) is supported by microprobe analyses recently published by Iijima and Matsumoto (1982). These authors argue that berthierine forms in diagenetic reactions within the 60 to 150 °C range at the expense of kaolinite and siderite. At higher temperatures (above 160 °C) both berthierine and any residual kaolinite are rendered unstable relative to 14 Å chamosite or pyrophyllite. The latter reaction is obviously consistent with grain-coating chlorite development in sandstones.

It has been tentatively suggested that swelling chlorites represent an intermediate stage within a diagenetic progression from trioctahedral smectite to chlorite. Smectites are common early hydration products of glass in volcanclastic sediments (Davies *et al.*, 1979, for example) yet do not survive deep burial. To our knowledge, however, no systematic and detailed investigation of smectite alteration with depth in volcaniclastic sediments has been undertaken.

Conclusions

We have presented new chemical data for a range of authigenic sedimentary chlorite minerals. Grain-coating chlorites in sandstones differ from metamorphic chlorites in being mostly polytype *Ib*

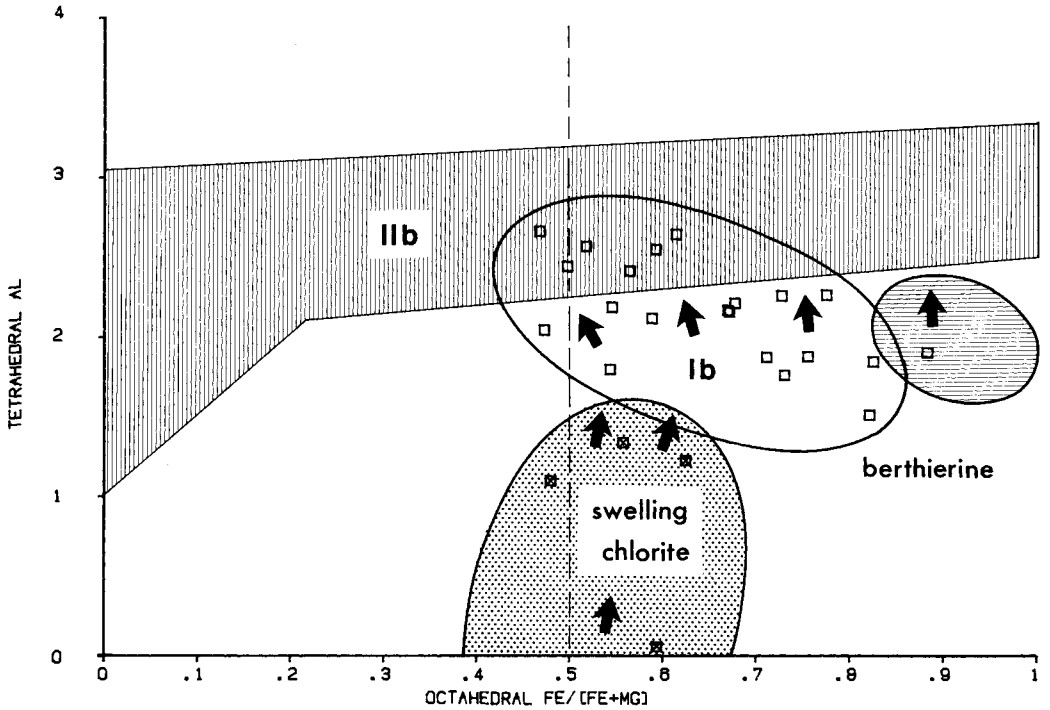

FIG. 8. Possible evolutionary pathways linking different chlorite varieties.

($\beta = 90\,°C$) and confined to the Fe-rich end of the Mg/Fe substitutional range. They also tend to be more siliceous (lower tetrahedral Al) as can be seen in the summary diagram, fig. 8.

Berthierines appear to have broadly similar chemical compositions although with very high Fe/Mg ratios. Swelling chlorites are more magnesian and, when presented in the form of chlorite formulae, have much higher silica contents and lower octahedral cation totals. Both can be attributed to substantial smectite interstratification. It is also possible that the *Ib* ($\beta = 90°$) polytype field in fig. 8, and the 'anomalous' Al-poor chlorites in Foster's (1962) data, plot where they do because of minor (residual?) smectite interstratifications. Structural reorganization to polytype *IIb* would presumably eliminate these and hence account for differences in composition between diagenetic and metamorphic chlorites.

Implicit in fig. 8 are several possible evolutionary pathways. Swelling chlorites develop from smectites and, with increasing depth of burial, are converted first to polytype *Ib* then, with the transition to metamorphism, polytype *IIb*.

The work of Iijima and Matsumoto (1982) has shown that berthierines are transformed to 14 Å chlorites during deep burial diagenesis. Presumably these, too, recrystallize to polytype *IIb* at higher temperatures.

The best-described diagenetic chlorites, however, do not seem to develop by either of these mechanisms. Grain coating chlorites in sandstones form at intermediate burial depths and their delicate and distinctive morphology suggests growth from solutes in pore-water, not by replacement of some precursor phase. Other diagenetic reactions accompanying chlorite formation are destruction of kaolinite and certain carbonate minerals and (mostly in shales) illitization of smectite and illite/smectite clay minerals.

Fe^{2+} and Mg^{2+} released from the illitization reaction are thought to be the key reactants according to Boles and Franks (1979):

$$3.5Fe^{2+} + 3.5Mg^{2+} + 3Al_2Si_2O_5(OH)_4 + 9H_2O \rightarrow (Fe_{3.5}Mg_{3.5}Al_4)[Al_2Si_6O_{20}](OH)_{16} + 14H^+.$$

Iijima and Matsumoto (1982) argued for reaction of kaolinite with siderite to produce berthierine:

$$9FeCO_3 + 3Al_2Si_2O_5(OH)_4 + 2H_2O \rightarrow (Fe_9Al_3)[Al_3Si_5O_{20}](OH)_{16} + SiO_2 + 9CO_2.$$

Both of these reactions generate acid which has implications for the stability of other phases present. Another possible source of Fe, however, is

oxidized iron (hematite, goethite). Reduction to Fe^{2+} causes an increase in alkalinity:

$$2Fe_2O_3 + C + 4H_2O \rightarrow 4Fe^{2+} + HCO_3^- + 7OH^-.$$

Berthierine or chamosite formation need not, therefore, increase pore-water acidity greatly.

$$5Fe_2O_3 + 2Al_2Si_2O_5(OH)_4 + 2SiO_2 + 4H_2O + 2.5C \rightarrow (Fe_{10}Al_2)[Al_2Si_6O_{20}](OH)_{16} + 2.5CO_2.$$

Additional iron reduction would favour carbonate co-precipitation (ankerite?) with no increase in acidity (Curtis, 1985).

The chlorite structure is stable over a wide range of both diagenetic and metamorphic environments. The bulk composition of sediments and reactivity of common sedimentary minerals is such that diagenetic chlorites tend to be Fe rich. The progression from diagenesis to metamorphism seems to be characterized by polytype change (Hayes, 1970) and some compositional modification. The latter may well be due to elimination of minor smectite interstratifications.

Acknowledgements. This work was funded by the Natural Environment Research Council (including a research studentship: CKW), the Science and Engineering Research Council and the Amoco Production Company, Tulsa Research Centre. Samples were supplied by Amoco, Exxon and BP and this provision is gratefully acknowledged. Many people assisted with the work at various stages: Alan Sheldon, Sarah Curtis, and Susan Forster in particular helped with microscopy, computing, and manuscript preparation respectively. An anonymous reviewer made very helpful suggestions.

REFERENCES

AIPEA (1980) *Clays Clay Minerals*, **28,** 73–8.
Bailey, S. W. (1980) In *Crystal structures of clay minerals and their X-ray identification* (G. W. Brindley and G. Brown, eds.). Mineralogical Society, London, p. 495.
——and Brown, B. E. (1962) *Am. Mineral.* **47,** 819–50.
Boles, J. R., and Franks, S. G. (1979) *J. Sediment. Petrol.* **49,** 55–70.
Brindley, G. W. (1961) In *The X-ray identification and crystal structures of clay minerals* (G. Brown, ed.). Mineralogical Society, London, p. 544.
Curtis, C. D. (1985) *Phil. Trans. R. Soc. London*, A. In press.
——Ireland, B. J., Whiteman, J. A., Mulvaney, R., and Whittle, C. K. (1984) *Clay Minerals*, **9,** 471–81.
Davies, D. K., Almon, W. R., Bonis, S. B., and Hunter, B. E. (1979) *S.E.P.M. special publication no.* 26, 281–306.
Deer, W. A., Howie, R. A., and Zussman, J. (1962) *Rock-forming minerals*, **3.** Longmans, London, 270 pp.
Foster, M. D. (1962) *U.S.G.S. Prof. Paper* 414-A, 33 pp.
Griffin, J. J., Windom, H., and Goldberg, E. D. (1968) *Deep Sea Research*, **15,** 433–59.
Hayes, J. B. (1970) *Clays Clay Minerals*, **18,** 285–306.
Hutcheon, I., Oldershaw, A., and Ghent, E. D. (1980) *Geochim. Cosmochim. Acta*, **44,** 1425–35.
Iijima, A., and Matsumoto, R. (1982) *Clays Clay Minerals*, **30,** 264–74.
Ireland, B. J., Curtis, C. D., and Whiteman, J. A. (1983) *Sedimentology*, **30,** 769–86.
McDowell, S. D., and Elders, W. A. (1980) *Contrib. Mineral. Petrol.* **74,** 293–310.
MacEwan, D. M. C. and Wilson, M. J. (1980) In *Crystal structures of clay minerals and their X-ray identification* (G. W. Brindley and G. Brown, eds.). Mineralogical Society, London, pp. 495.
Muffler, L. P. J., and White, D. E. (1969) *Geol. Soc. Am. Bull.* **80,** 157–82.
Parry, W. T., and Downey, L. M. (1982) *Clays Clay Minerals*, **30,** 81–90.
Phakey, P. P., Curtis, C. D., and Oertel, G. (1972) Ibid. **20,** 193–7.

[*Manuscript received 10 May 1984; revised 16 September 1984*]

(*See following page for Appendix*)

APPENDIX: samples studied

A02:	TUSCALOOSA SANDSTONE (L. Cretaceous)	5608.2 m
	Medium-grained litharenite	(10 analyses)
A03:	TUSCALOOSA SANDSTONE (L. Cretaceous)	5609.1 m
	Medium-grained lithic arkose	(18 analyses)
A04:	TUSCALOOSA SANDSTONE (L. Cretaceous	5610.2 m
	Medium-grained lithic arkose	(31 analyses)
A05:	TUSCALOOSA SANDSTONE (L. Cretaceous)	5611.7 m
	Medium-grained feldspathic litharenite	(26 analyses)
A06:	TUSCALOOSA SANDSTONE (L. Cretaceous)	2406.3 m
	Fine-grained lithic arkose	(18 analyses)
A07:	TUSCALOOSA SANDSTONE (L. Cretaceous)	2407.2 m
	Fine-grained lithic arkose	(8 analyses)
A10:	ALASKAN SANDSTONE (Cretaceous)	Depth unknown
	Fine-grained feldspathic litharenite	(37 analyses)
A11:	ALASKAN SANDSTONE (Palaeogene)	Depth unknown
	Coarse-grained arkose	(66 analyses)
A12:	BELLY RIVER SANDSTONE (U. Cretaceous)	1240.6 m
	Medium-grained feldspathic litharenite	(16 analyses)
A13:	BELLY RIVER SANDSTONE (U. Cretaceous)	1192.9 m
	Medium-grained feldspathic litharenite	(7 analyses)
A14:	BELLY RIVER SANDSTONE (U. Cretaceous)	994.4 m
	Medium-grained feldspathic litharenite	(20 analyses)
A15:	BELLY RIVER SANDSTONE (U. Cretaceous)	1000.7 m
	Coarse-grained feldspathic litharenite	(19 analyses)
A17:	FALHER FORMATION (L. Cretaceous)	1896.0 m
	Fine-grained litharenite	(15 analyses)
A21:	FALHER FORMATION (L. Cretaceous)	1978.3 m
	Fine-grained litharenite	(17 analyses)
B01:	NORTH SEA SANDSTONE (Age unknown)	3574.5 m
	Fine-grained arkose	(33 analyses)
B07:	NORTH SEA SANDSTONE (Age unknown)	3577.0 m
	Fine-grained lithic arkose	(26 analyses)
B08:	NORTH SEA SANDSTONE (Age unknown)	3552.8 m
	Medium-grained lithic arkose	(17 analyses)
B09:	NORTH SEA SANDSTONE (Age unknown)	3576.5 m
	Fine-grained lithic arkose	(22 analyses)
B10:	NORTH SEA SANDSTONE (Age unknown)	3577.5 m
	Fine-grained lithic arkose	(14 analyses)
B16:	NORTH SEA SANDSTONE (Age unknown)	3561.9 m
	Fine-grained lithic arkose	(25 analyses)
FRD:	FRODINGHAM IRONSTONE (L. Jurassic)	Surface
	Chamosite-oolite-siderite 'ironstone'	(17 analyses)
058:	HAMERSLEY GROUP (L. Proterozoic, 2.6 Ga)	199.6 m
	Mt. McCrae shale	(43 analyses)
065:	HAMERSLEY GROUP (L. Proterozoic, 2.6 Ga)	214.9 m
	Mt. McCrae shale	(36 analyses)
P45:	DALES GORGE MEMBER, HAMERSLEY GROUP (L. Proterozoic, 2.6 Ga)	Near-surface
	Banded iron formation	(26 analyses)
BL1R:	LOWER SLATE SERIES/CAERNARFON SLATE BELT (L. Cambrian)	Surface
	Purple/red slates	(6 analyses)
BL2G:	LOWER SLATE SERIES/CAERNARFON SLATE BELT (L. Cambrian)	Surface
	Purple/red slates - reduction spot	(5 analyses)